Dual Enzyme-like Performances of PLGA Grafted Maghemite Nanocrystals and Their Synergistic Chemo/Chemodynamic Therapy for Human Lung Adenocarcinoma A549 Cells

Xueqin Wang (wangxq0708@163.com)
Henan University of Technology https://orcid.org/0000-0001-8744-850X
Miao Cui
Henan University of Technology
Fan Ouyang
Henan University of Technology
Yuqi Guo
Henan Provincial People's Hospital
Ruifang Li
Henan University of Technology
Shaofeng Duan
Henan university
Tiandi Xiong
Henan University of Technology
Huiru Zhang
Henan University of Technology
Yunlong Wang
Henan Bioengineering Research Center

Research

Keywords: Maghemite nanoparticles, POD- and CAT-like activity, Reactive oxygen species, Lung adenocarcinoma A549 cells

Posted Date: November 19th, 2020

DOI: https://doi.org/10.21203/rs.3.rs-108083/v1

Dual enzyme-like performances of PLGA grafted maghemite nanocrystals and their synergistic chemo/chemodynamic therapy for human lung adenocarcinoma A549 cells

Xueqin Wang[1], Miao Cui [1], Fan Ouyang [1], Yuqi Guo[3], Ruifang Li[1], Shaofeng Duan[4]*, Tiandi Xiong[1], Huiru, Zhang[1]*, Yunlong Wang[2]*

[1] *College of Bioengineering, Henan University of Technology, Zhengzhou, Henan 450001, P.R. China ;* [2]*Henan Bioengineering Research Center, Zhengzhou, 450046, P.R.China;* [3]*Henan Provincial People's Hospital, Zhengzhou 450003, P.R. China;* [4]*School of Pharmacy, Henan University, Kaifeng, Henan 475004, P.R. China.*

** Corresponding authors: Shaofeng Duan, Tel: + 86 371 22822134, E-mail address: sduan@henu.edu.cn, School of Pharmacy, Henan University, Kaifeng, Henan 475004, P.R. China; Huiru, Zhang, Tel: + 86 371 67756317, E-mail address: zhr67@163.com, College of Bioengineering, Henan University of Technology, Zhengzhou, Henan 450001, P.R. China; Yunlong Wang, Tel: + 86 371 67999699, E-mail address: biowyl@126.com, Henan Bioengineering Research Center, Zhengzhou, 450018, P.R.China.*

Abstract

Advancing nanocatalytic therapies of tumors formed on non-toxic but catalytically active inorganic nanoparticles (NPs) have aroused great interest in tumor therapy recently, but the limited reactive oxygen species within tumors may limit treatment efficiency. Therefore, the combination of chemotherapy and chemodynamic therapy is a promising treatment strategy. Herein, poly(lactic

acid-*co*-glycolic acid) (PLGA) grafted-γ-Fe_2O_3 nanoparticles (NP_{PLGA}) with dual response of endogenous peroxidase (POD)- and catalase (CAT)-like activities has been reported. On the one hand, the NP_{PLGA} could serve as a drug delivery system for doxorubicin (DOX), an anti-tumor drug used to treat lung adenocarcinoma A549 cells. On the other hand, based on the mimetic enzyme properties of NP_{PLGA}, it can be combined with DOX to treat lung cancer. The results show that the NP_{PLGA} could be simulated the CAT-like activity to decompose hydrogen peroxide (H_2O_2) into H_2O and O_2 under neutral tumor microenvironment, so as to reduce the oxidative damage caused by H_2O_2 to lung adenocarcinoma A549 cells. Under acidic microenvironment, NP_{PLGA} could simulate POD-like activity to effectively catalyze the decomposition of H_2O_2 to produce highly toxic hydroxyl radicals (•OH) to induce the death of tumor-cell through regular catalytic reaction of Fenton. Furthermore, the POD-like activity of NP_{PLGA} synergistic with DOX can promote the apoptosis and destruction of A549 cells and enhance the antitumor impact of DOX-NP_{PLGA}. Therefore, this study provides an efficacious dual inorganic biomimetic nanozyme-based nanoplatform for lung tumor treatment.

Keywords: Maghemite nanoparticles, POD- and CAT-like activity, Reactive oxygen species, Lung adenocarcinoma A549 cells

Introduction

Recently, chemodynamic therapy (CDT) formed on nontoxic but catalytically active inorganic nanozymes for intratumoral generation of high-toxic reactive oxygen species (ROS) has been

widely studied in tumor therapy due to its high specificity and diminished invasiveness [1]. Within the period of the CDT procedure, endogenous hydrogen peroxide (H_2O_2) is decomposed into ROS and hydroxyl radicals (·OH) through the medium acidic tumor microenvironment (TME) by an intratumoral Fenton or Fenton-like reaction by metal catalysts (e.g., Fe, Mn, Cu, etc.). Nanozyme is a kind of nanomaterial with natural mimic enzyme catalytic activity [2,3]. As a new generation of artificial enzyme, nanoenzyme has the advantages of simple synthesis [4], adjustable catalytic activity [5,6], high stability, low cost and easy operation [7,8]. They have become a promising alternative to natural enzymes and have attracted extensive exploration by biomedical researchers [9-11].

Maghemite (γ-Fe_2O_3) and magnetite (Fe_3O_4) nanoparticles (NPs) are two main iron oxide nanoparticles (IONPs) that are often utilized in a diversity of biomedical functionalities, including magnetic targeting and drug/gene delivery [12-14], tumor therapy [15, 16], magnetic resonance imaging [17, 18], cell labeling and isolation [19-21], magnetic biosensors [22, 23], and magnetic hyperthermia [24, 25]. However, ferrous Fe_3O_4 may increase the risk of toxicity and chemical instability [26, 27]. Therefore, γ-Fe_2O_3 can be used as a good candidate for long-term biomedical and clinical applications. Recently, it has been reported that Fe_3O_4 and γ-Fe_2O_3 NPs have intrinsic enzyme simulation activity and have been developed as catalysts for Fenton reaction, which can catalyze the formation of •OH in situ H_2O_2 in solid tumors, thus leading to the death of cancer cells [28-30]. Moreover, Fe_3O_4 and γ-Fe_2O_3 NPs showed pH-dependent peroxidase (POD)-like as well as catalase (CAT)-like performances [31,32]. A typical example of its inherent POD-like activity is that IONPs is able to catalyze the POD oxidation substrates when H_2O_2 is available in acidic solutions to generate blue products [28]. Mechanism studies have shown that IONPs initially reduce

H_2O_2 to create •OH, which then organizes the oxidation of the studied substrate [33-35]. Dissimilar with the natural POD, IONPs mostly lost POD-like performance at neutral pH. However, we found that γ-Fe_2O_3 NPs directly catalyzed H_2O_2 to generate H_2O and oxygen (O_2) under such a condition, which is called CAT-like activity, and can protect cells from the stress of oxidative damage in this study [36].

In the process of cell metabolism, O_2 undergoes a series of single-electron reduction to form ROS, including O_2^-, O_2^{2-}, ·OH, ·OOH radicals, H_2O_2, etc [37]. Low-dose ROS play an important role in cell proliferation, signal transduction, differentiation, migration, and body's resistance to the invasion of pathogen [37]. Although, unusually increased ROS levels will devastate the redox homeostasis, result in oxidative stress, and seriously harm the function and infrastructure of cellular macromolecules. The systems of enzyme including glutathione peroxidase (GPx), superoxide dismutase (SOD), and CAT protect cells from ROS damage by regulating intracellular ROS levels. Nanozyme can also regulate intracellular ROS levels [38,39]. The ROS scavenging ability of nanozyme mainly comes from the simulation activity of SOD, which converts superoxide into H_2O_2 and then into O_2 and H_2O, thus reducing intracellular ROS level and enhancing cell activity. ROS is produced by converting H_2O_2 into •OH free radicals through its POD-like activity. The reaction of iron-mediated Fenton turns endogenous H_2O_2 into highly toxic •OH, leading to irreversible oxidative damage against tumor cells.

CDT-based Fenton reaction has been proposed as an efficacious strategy for treatment of cancers. However, the limited H_2O_2 concentration in tumor cells severely limits the efficacy of CDT [40]. Thus, combining with CDT with other therapeutic methods, including chemotherapy [40], and photothermal treatment [41], is a marvelous way to improve the anticancer impact. Here, we

combined CDT with chemotherapy drug DOX to effectively treat lung adenocarcinoma A549 cells. As shown in Scheme 1, NP_{PLGA} was first prepared with superparamagnetic γ-Fe_2O_3 NPs as the core, followed by the surface modification with poly (lactic-*co*-glycolic acid) (PLGA) and the loading of the chemotherapy drug DOX. This formed nanocatalyst drug DOX-NP_{PLGA}, through a reaction similar to Fenton under acidic TME, will show POD-like activity, produce highly toxic •OH, induce the death of cancer A549 cells, augment the sensibility of A549 cells to DOX, and enhance the therapeutic effect of CDT. In the neutral TME, the nanocatalyst exhibited CAT-like activity and could decompose H_2O_2 into H_2O and O_2, thus reducing the oxidative damage of H_2O_2 to A549 cells. Furthermore, the synergistic anti-tumor effect and related mechanism of NP_{PLGA} and DOX-NP_{PLGA} on A549 cells were further studied in detail.

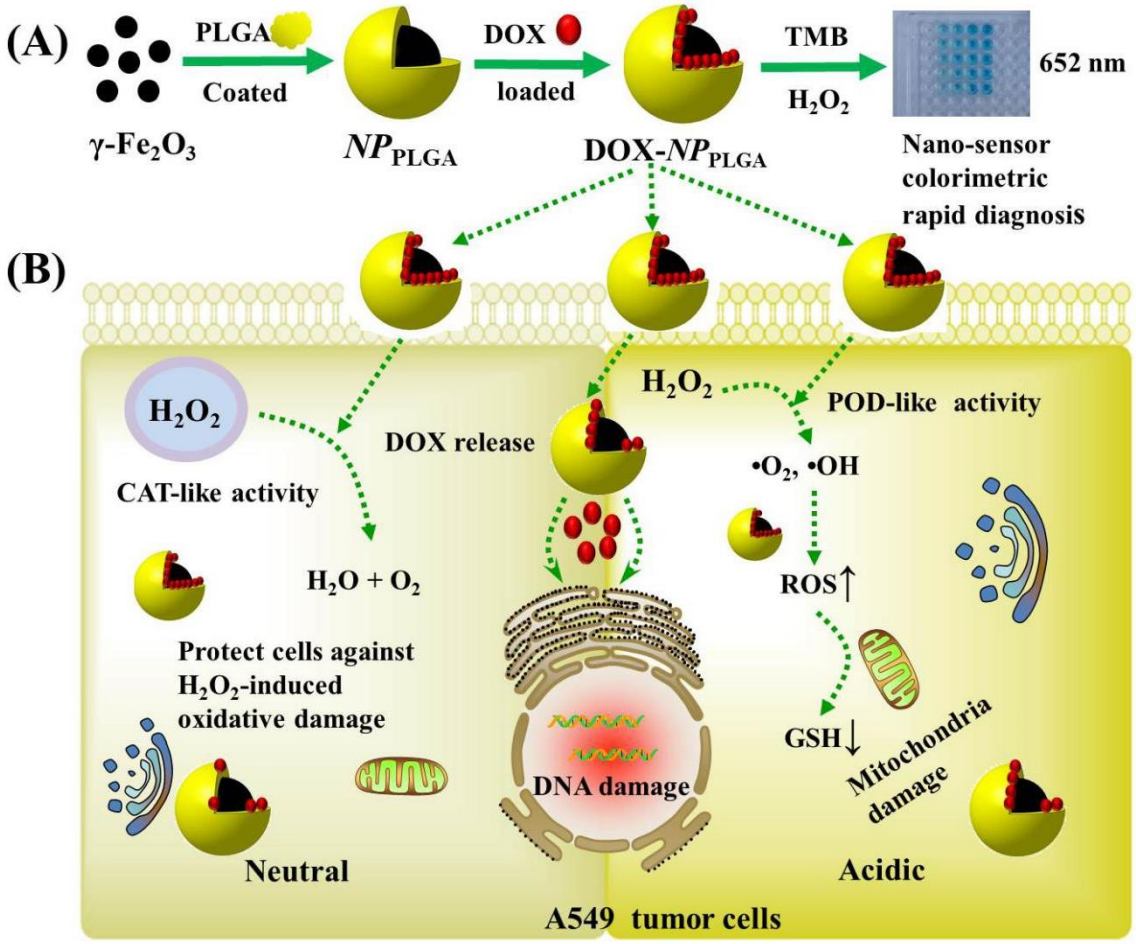

Scheme. 1 Schematic diagram of the functional pattern of DOX-NP_{PLGA} and its enhanced anti-tumor effect. **A** Preparation of DOX-loaded NP_{PLGA} and colorimetric determination in lung adenocarcinoma A549 cells. **B** In a neutral TME, DOX-NP_{PLGA} displayed CAT-like activity by decomposing H_2O_2 into H_2O and O_2. In an acidic TME, DOX-NP_{PLGA} released DOX and exhibited POD-like activity to produce highly toxic •OH, which caused the growth of ROS accumulation as well as the decrease of GSH in tumor A549 cells, and the further synergistic effect with DOX, causing efficient cell death.

Experimental

Materials

Human lung adenocarcinoma A549 cells was from the Shanghai Cell Bank of the Chinese Academy of Sciences (Shanghai, China). CAT from the liver of bovine (2000−5000 U mg^{-1}), POD from horseradish VI (250−330 U mg^{-1}). The RPMI-1640 cell culture medium and fetal bovine serum (FBS) were from Gibco Invitrogen Corporation (CA, USA). PLGA (lactide/glycolide molar ratio of 50: 50, MW=7000–17,000), 3-(4,5-dimethylthiazol-2-diphenyl-tetrazolium) bromide (MTT), 3,3',5,5'-tetramethylbenzidine (TMB), H_2O_2, potassium ferrocyanide (Perls reagent), dimethyl sulfoxide (DMSO), Hoechst 33258, Triton X-100 solution, and paraformaldehyde were obtained from Sigma-Aldrich (St. Louis, MO,USA). DOX was purchased from Aladdin Bio-Chem Technology Co., Ltd (Shanghai, China). Fluorescent dye FITC and 4, 6 diamidino-2-phenylindole (DAPI) were obtained from Molecular Probes, Inc. (Eugene, OR, USA). ROS assay and Annexin V-FITC apoptosis assay kits were obtained from Keygen Biotech Co., Ltd. (Nanjing, China). CAT assay and reduced glutathione (GSH) assessment kits were obtained from solarbio science and

technology Co., Ltd (Beijing, China). Other chemicals and specimens were from local commercial providers and the grade of the analytical reagents, unless otherwise mentioned.

Synthesis and characterization of NP_{PLGA}

The magnetic γ-Fe_2O_3 NPs were synthesized by chemical coprecipitation method [42,43], then PLGA was grafted to prepare NP_{PLGA}. The morphology, size, crystal structure and stability of γ-Fe_2O_3 NPs and NP_{PLGA} were characterized in our previous study [44].

The dual POD-like and CAT-like activity of NP_{PLGA}

In our previous work, the POD-like activity and steady-state kinetics of NP_{PLGA} were studied in detail [44]. The CAT-like performance of NP_{PLGA} was evaluated by CAT assessment kit conforming to the protocols of the manufacturer. In brief, 10 μL of NP_{PLGA} solution (1 mg mL^{-1}) or CAT solution (1 mg mL^{-1}) was added to 50 μL buffer (T-S buffer, 33 mM phosphoric acid, 33 mM citric acid, 23 mM boric acid, pH 7.0) when H_2O_2 is available at different concentrations. After 5 min of reaction, the dilution of residual H_2O_2 was performed 50 times with T-S buffer solution and detected with 520 nm UV-VIS spectrophotometer (UV-1000, Shanghai, China). The kinetic parameters of NP_{PLGA} were assessed utilizing the following the plot of Lineweaver-Burk (a):

$$\frac{1}{V} = \frac{1}{V_{max}} + \frac{K_m}{(V_{max}S)} \quad \text{(a)}$$

Where V states the primary velocity, V_{max} represents the maximum velocity of reaction, S represents the concentration of the substrate, and K_m states the constant of Michaelis-Menten, which is equal to the concentration of substrate at which the conversion rate is half of V_{max} and represents the enzyme affinity [45]. V_{max} was measured as the molar alternation by the absorbance of UV

based on the following Eq. (b):

$$A = \varepsilon lc \quad \text{(b)}$$

Further, A represent the absorbance, ε shows the coefficient of absorbance, l shows the distance length, and c represents the molar concentration with $\varepsilon = 3.9 \times 10^4\ M^{-1}cm^{-1}$ and $l = 10$ mm [46].

DOX loading and determination of encapsulation efficiency

500 µL of solution of DOX (2 mg mL^{-1}) was blended with 1000 µL of NP_{PLGA} solution (1 mg mL^{-1}), well-stirred for 1 h, and then rinsed three times with deionized (DI) water. The loading of DOX content was determined utilizing a UV-VIS spectrophotometer (UV-1000, Shanghai, China) with the absorbance at 480 nm. The content of drug loading was determined as the amount of loaded drug (mg) for every 100 mg of polymeric nanoparticles, whilst the efficiency of encapsulation was determined through the encapsulated ratio of drug to the primary amount of drug.

$$\text{Loading content } (\%) = \frac{W_t}{W_s} \times 100\%$$

$$\text{Encapsulation efficiency } (\%) = \frac{W_t}{W_o} \times 100\%$$

Where W_t shows the weight of DOX in NP_{PLGA}, W_s states the weight of NP_{PLGA}, and W_0 represents the primary weight of DOX in the procedure.

Cell culture and cytotoxicity assessment

The lung adenocarcinoma A549 cells were routinely cultured in an RPMI–1640 medium including

1% streptomycin (100 μg mL^{-1}), 1% penicillin (100 U mL^{-1}) and 10% heat-inactivated FBS, in a humidified incubator at 37 ℃ with an atmosphere of 95% air and 5% CO_2. The cells were typically passaged at a ratio of 1:3 every 3 days to retain the growth stage exponentially.

After A549 cells reached the exponential growth stage, the cells were harvested to provide cell suspension. Subsequently, the cells were inoculated into microwell containing 96-well with a density of 8,000 cells per well. After 12 h of incubation, the cells were processed with NP_{PLGA} at various concentrations (50, 100, 200, and 400 μg·mL^{-1}). After 12 h of co-incubation, 20 μL MTT solution (5 mg·mL^{-1}) was added to the wells. Following 4 h of incubation, the culture media was taken out and the dissolution of formed formazan in 150 μL of DMSO was performed. The microwell plate was incubated for 15 min again. At last, the wells absorbance was assessed at 490 nm with a microporous plate spectrophotometer (Infinite F200, Tecan Group Ltd., Switzerland).

MTT assessment was performed to detect the effect of NP_{PLGA} on oxidative damage of A549 cells under different pH conditions induced by H_2O_2. Briefly, A549 cells were cultured for 24 h in a different medium (pH 7.4 or pH 6.0) and then treated with various concentrations of NP_{PLGA} (50, 100, 200, 400 μg·mL^{-1}) in A549 cells for 12 h. The medium was then eliminated, rinsed with PBS once, continued with the addition of 1 mM or 5 mM H_2O_2. The cells were then incubated for 30 min at 37 ℃ containing 5% CO_2. The viability of the treated cells was specified through MTT assessment. Additionally, MTT was used to evaluate the H_2O_2-induced oxidative damage within A549 cells using different formulation treatments.

Analysis the levels of intracellular ROS

The levels of ROS in A549 cells treated with different formulations were determined using the ROS

test kit following the protocols of manufacturer. A549 cells were first processed for 12 h with 200 μg·mL^{-1} NP_{PLGA}, and then rinsed with PBS and incubated for 15 min with 50 μM DCFH-DA in FBS-free RPMI 1640 media at 37 ℃ in the dark. Further, after the cells were rinsed two times with PBS, the group cultured in the medium at PH 7.4 was treated for 20 min with 5 mM H_2O_2, and the group cultured in the medium at pH 6.0 was treatment with 1mM H_2O_2 for 10 min. The cells were washed again, and the levels of intracellular ROS were evaluated *via* the microscope of inverted fluorescence (Eclipse TE 2000-U) supplied with a high-resolution CCD camera (CVS3200).

Detection of GSH in the treated A549 cells

A549 cells were implanted in a cultrue plate containing 6 wells at a cell density of 1 × 10^6 cells per well and incubated for at 37 ℃12 h. Subsequently, 200 μg/mL NP_{PLGA} or 100 μg/mL DOX-NP_{PLGA} was used for treating the cells and procedure continued by for 12 h of incubation in an acidic medium. Later, 1 mM H_2O_2 was added for another 10 min of incubation. The treated cells were then gathered and rinsed with PBS for three times, and then resuspended in PBS by adding the triple volume of the cell pellet. After 3 times of freezing and thawing, the cells were centrifuged for 10 min at 8000 g, and the supernatant was gathered at 4 ℃. Subsequently, the supernatant was detected using a reduced GSH kit according to the manufacturers' instructions. The absorbances at 450 nm were detected immediately utilizing the spectrophotometer (Infinite F200, Tecan Group Ltd., Switzerland).

Apoptosis assessment

To assess the apoptotic cells, A549 cells processed with different formulations were stained with the solution of Hoechst H33258 (2 μg mL^{-1}) at room temperature (RT) for 10 min. The stained cells

were observed using an inverted fluorescence microscope, and unprocessed A549 cells utilized as the control.

Apoptosis was quantitatively evaluated by the assessment kit of Annexin V-FITC apoptosis (Keygen Biotech, Nanjing, China). The Annexin V-FITC-PI double labeling was conducted conforming to the kit manual of manufacturer. The A549 cells processed with different formulations were gathered and rinsed with PBS. Later, the staining of 1×10^6 cells were performed by 5 μL Annexin V-FITC and 5 μL PI in a 500 μL buffer of binding at RT for 15 min in the dark. Finally, the apoptotic cells were determined via flow cytometer of FACS Calibur (BD Biosciences, San Jose, CA) using untreated A549 cells as the control.

Results and discussion

Characterization of NP_{PLGA}

The core-shell structure of NP_{PLGA} can ensure the dispersion stability of γ-Fe_2O_3 NPs, enhance its enzyme-like activity (Fig. 1A), and improve the bio-compatibility of NP_{PLGA} for further intracellular application. The structure and morphology of the γ-Fe_2O_3 NPs and NP_{PLGA} were characterized employing the Fourier-transform infrared spectrum (FT-IR), transmission electron microscope (TEM), and X-ray diffractometer (XRD). The details can be found in our previous study [44]. The TEM images illustrated that the prepared nanoscale γ-Fe_2O_3 NPs had uniform morphology, the diameter range was 10-15 nm [44], and the NP_{PLGA} exhibited a mono-dispersed sphere with a 40-50 nm uniform size (Fig. 1B). Moreover, the XRD data demonstrated that the crystalline properties and the peaks conform to the standard γ-Fe_2O_3 reflection, but the α-Fe_2O_3 phase was not observed. Furthermore, these γ-Fe_2O_3 NPs were successfully modified by PLGA according to the FT-IR data

[44].

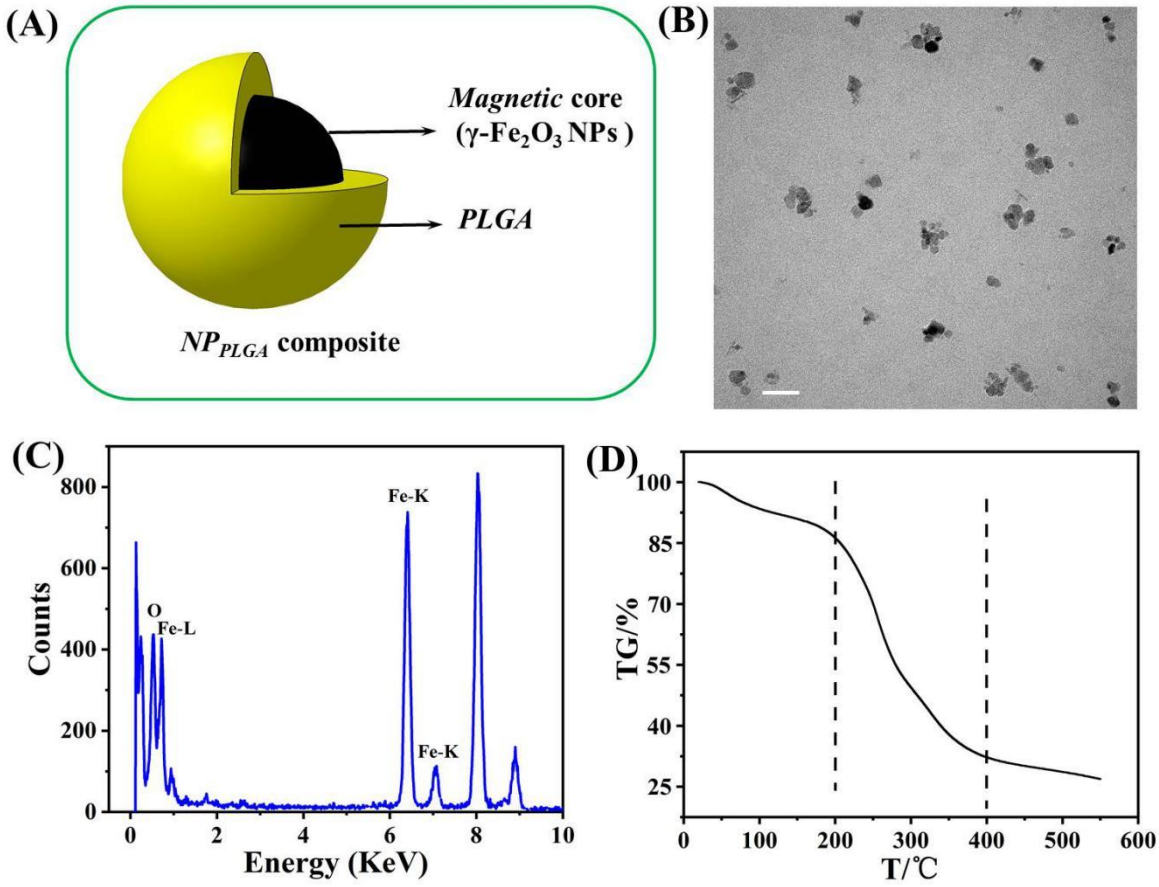

Fig. 1 **A** Schematic illustration of the composite NP_{PLGA}. **B** TEM image of NP_{PLGA}. Scale bar = 50 nm. **C** EDS spectrum of NP_{PLGA}. **D** Thermogravimetric curve of NP_{PLGA}.

To accurately analyze the elements of the NP_{PLGA}, EDS spectroscopy characterization was performed to confirm the presence of O and Fe (Fig. 1C). Thermogravimetric analysis was used to determine the change of NP_{PLGA} mass with temperature increase. The results showed that the weight loss of NP_{PLGA} was severe at 200-400℃, nearly 70% at 400℃, and stable at 550℃ at about 28.8% (Fig. 1D).

Dual enzyme-like catalytic activity of NP_{PLGA}

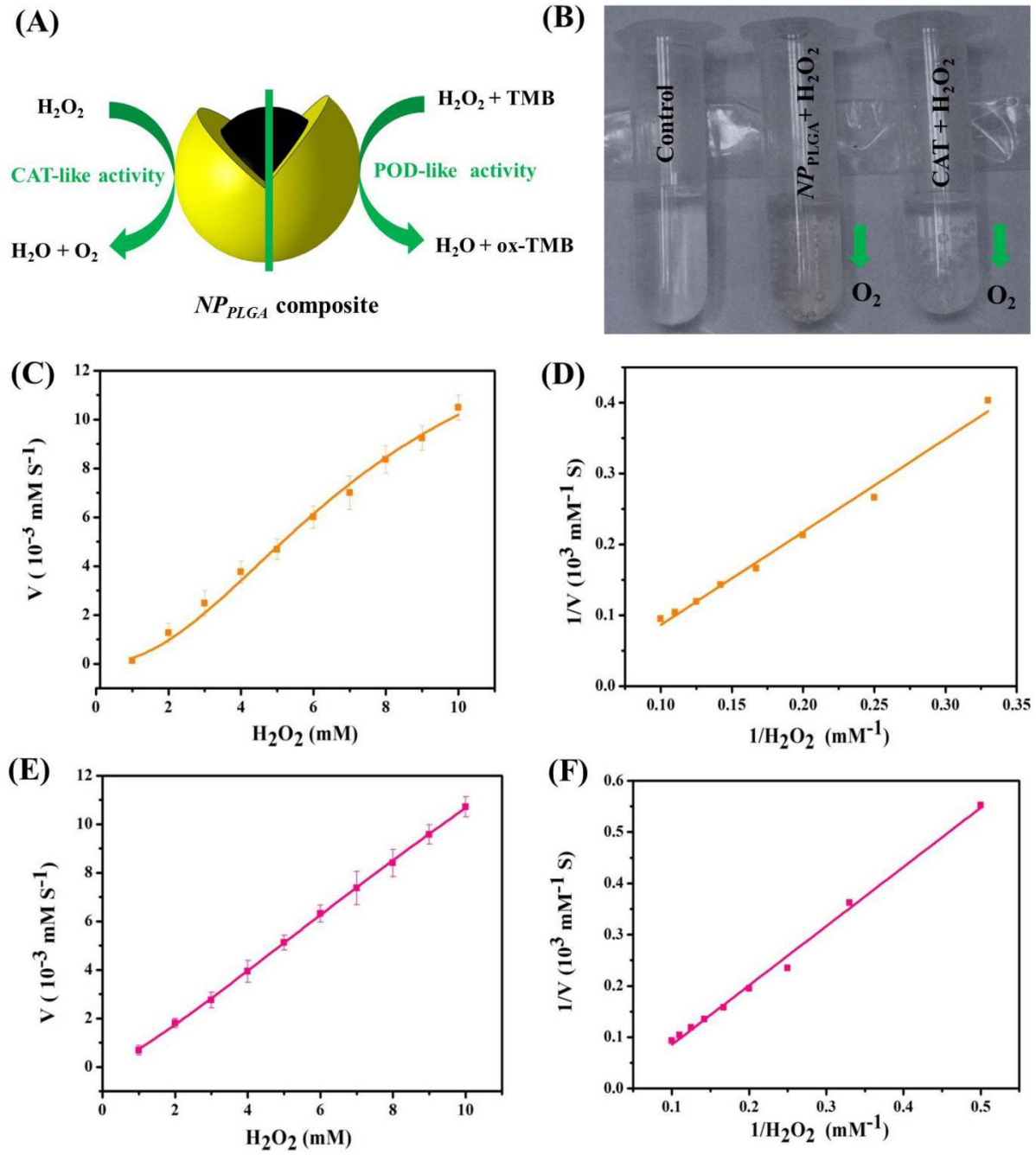

Fig. 2 A Schematic illustration for dual enzyme-like catalytic performance of the *NP*PLGA. **B** CAT-like activity assay of *NP*PLGA, both *NPPLGA* and natural CAT can catalyze H_2O_2 to produce O_2 when H_2O_2 is available in the system. **C** Steady-state Kinetic assays for *NPPLGA* in the presence of H_2O_2, and **D** corresponding double-reciprocal plot. E) Kinetic assays of natural CAT in the presence of H_2O_2, and F) corresponding double-reciprocal plot.

The POD-like activity and steady-state kinetic parameters of the NP_{PLGA} for TMB oxidation were studied in detail as we did previously [44]. The maximum primary velocity (V_{max}) and the contant of Michaelis−Menten (K_m) were measured utilizing the Lineweaver–Burk plot of the double reciprocal line related to the equation of the Michaelis–Menten. Kinetic analysis showed that NP_{PLGA} ($K_m = 0.9$) had a greater affinity for TMB compared to POD ($K_m = 1.98$) at acidic pH [44]. Furthermore, the outcomes revealed that for H_2O_2, the K_m value of NP_{PLGA} ($K_m = 4.41$) was greater than POD ($K_m = 0.30$), proposing that NP_{PLGA} needed a higher concentration of H_2O_2 to describe the same POD activity as natural POD.

We further examined the CAT-like activity of NP_{PLGA}. As shown in the Fig. 2B, it is obvious that O_2 was produced in the NP_{PLGA} and natural CAT groups when H_2O_2 is available, exhibiting that both NP_{PLGA} and natural CAT is able to catalyze H_2O_2 to create O_2. In order to measure the enzyme parameters, we investigated the steady-state kinetics of NP_{PLGA} through calculating the primary rates as a function of the concentration of H_2O_2. The catalytic procedure followed the normal Michiaelis-Menten reaction, and the Lineweaver−Burk diagram was shown in Fig. 2(C-F). As can be seen from Table 1, the K_m values of NP_{PLGA} and natural CAT were 0.76 mM and 0.86 mM, suggesting a high affinity of NP_{PLGA} to H_2O_2.

Table. 1 Michaelis–Menten (K_m) and maximum reaction velocity (V_{max})

Enzyme	**Substrate**	K_m **(mM)**	V_{max} **(10^{-3} mM s^{-1})**
Catalase (CAT)	H_2O_2	0.86	33.53
NP_{PLGA}	H_2O_2	0.76	22.32

Effect of CAT-like activity of *NP*$_{PLGA}$ on H_2O_2-induced cellular oxidative damage

We first evaluated the cytotoxicity of NP_{PLGA} to A549 cells by MTT assay, and A549 cells were processed for 24 h with various concentrations of NP_{PLGA}. The results indicated the processed A549 cells still maintained a high survival rate even when the concentration of NP_{PLGA} reached 400 $\mu g \cdot mL^{-1}$, indicating that NP_{PLGA} possessed a minor impact on the ability of A549 cell proliferation (Fig. 3A).

H_2O_2 is a common ROS produced in cellular metabolism, and CAT and POD have progressed to preserve cells against oxidative damage induced by H_2O_2 [47]. This study speculated that NP_{PLGA} with CAT-like activity had a protective effect on human lung cancer A549 cells against against oxidative damage induced by H_2O_2. MTT assessment was utilized to study the effect of NP_{PLGA} at different concentrations and 5 mM H_2O_2 on H_2O_2-induced oxidative damage of A549 cells in neutral TME. The results indicated that the rate of survival for A549 cells increased with the increase of NP_{PLGA} concentration (Fig. 3A). In addition, we further confirmed the effect of NP_{PLGA} on H_2O_2-induced oxidative damage of A549 cells with various treatments (Fig. 3B). The results suggested that the A549 cells co-treated with NP_{PLGA} and H_2O_2 displayed higher viability than those treated with H_2O_2 alone. This is because NP_{PLGA} could decompose H_2O_2 to generate H_2O and O_2 under neutral TME conditions, thereby reducing the toxicity and side effects on cells.

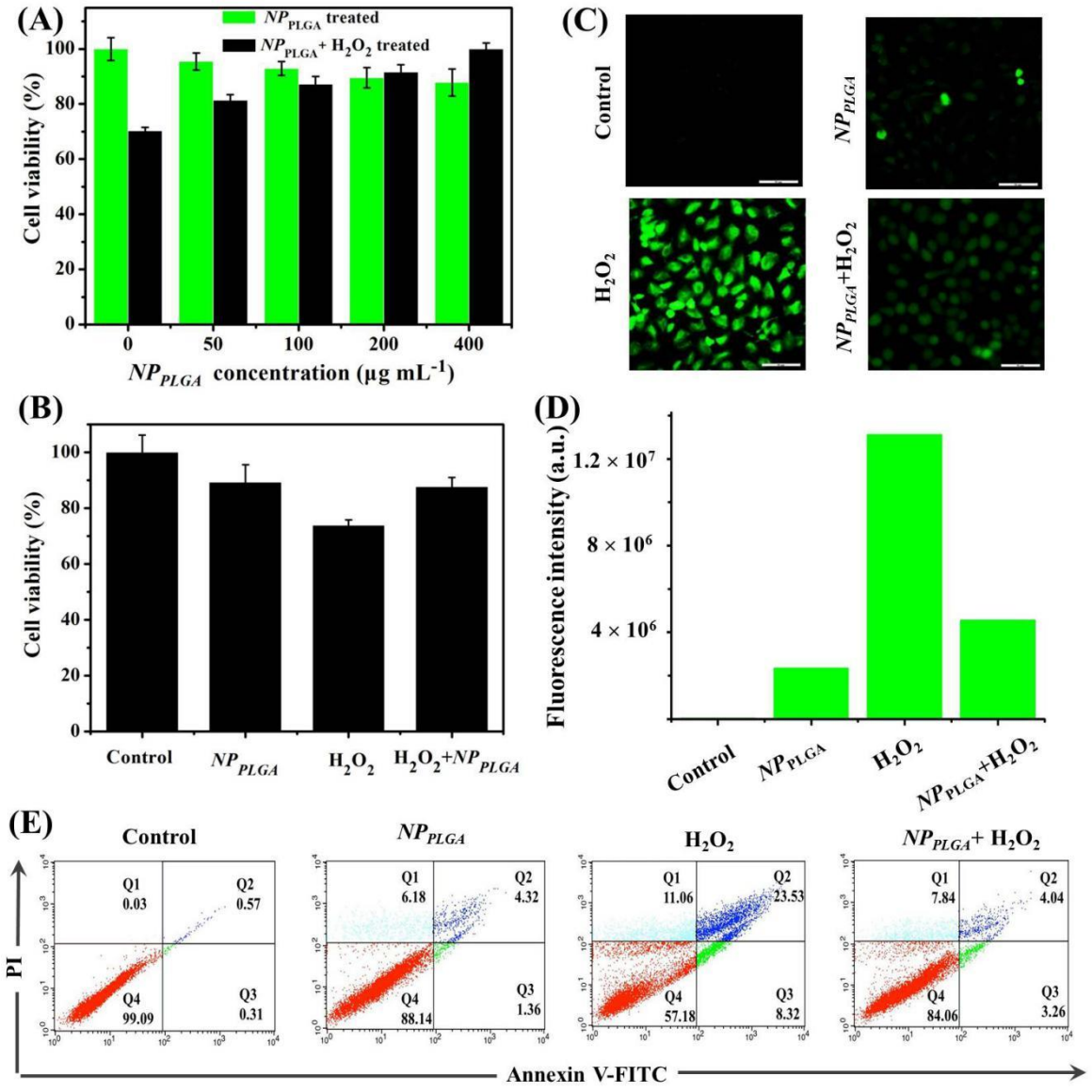

Fig. 3 A Cytotoxicity of NP_{PLGA} and H_2O_2-induced oxidative damage assays of treated A549 cells with various concentration of NP_{PLGA} including 50, 100, 200, 400 μg·mL^{-1}, and the cells were treated with various concentration NP_{PLGA} and 5 mM H_2O_2 under neutral TME conditions (pH 7.4). **B** H_2O_2-induced oxidative damage of A549 cells with different formulation treatments, the cells were treated for 12h, and the concentration of NP_{PLGA} was 200 μg·mL^{-1}. **C** Assays of ROS production in treated A549 cells for 12 h with different formulations, and **D** corresponding statistical of the fluorescence intensity analysis in the processed cells. **E** Apoptosis assays of the

processed A549 cells with different treatment through flow cytometry utilizing the staining methods of fluorescein Annexin V-FITC-PI double labeling, untreated A549 cells employed as a control. Early apoptosis (bottom right), late apoptosis (upper right), necrotic cells (upper left), and normal cells (bottom left).

We used a ROS fluorescence probe DCFH-DA to determine the intracellular ROS level. As shown in Figs. 3C and 3D, only weak green fluorescence was observed in the A549 cells treated with NP_{PLGA}. In contrast, bright green fluorescence signals was displayed in H_2O_2-processed cells, indicating upper intracellular ROS levels. However, cells treated with NP_{PLGA} and H_2O_2 showed relatively weak emission. These results illustrated that NP_{PLGA} was able to decompose H_2O_2, thus reducing the oxidative damage induced by H_2O_2. Furthermore, to survey the influence of H_2O_2-induced oxidative damage of NP_{PLGA} on the apoptosis of A549, flow cytometry was utilized to quantitatively evaluate the apoptosis level. It was displayed in the Fig. 3E, the number of normal cells reached about 90% after incubation for 12 h with 200 $\mu g \cdot mL^{-1}$ NP_{PLGA}, indicating that the cytotoxicity of NP_{PLGA} could be negligible. After treatment with 5 mM H_2O_2 for 20 min, more than half of A549 cells died. However, after treatment with NP_{PLGA} and H_2O_2 for 12 h, the cell activity was significantly enhanced, while the number of normal cells only increased to more than 80%. These results further confirmed that NP_{PLGA} could reduce the oxidative damage induced by H_2O_2.

Synergistic effect of POD-like activity of NP_{PLGA} combined with DOX on A549 cells

We first evaluated the sensitivity for A549 cells utilizing colorimetry based the POD-like activity of NP_{PLGA}. Various numbers of A549 cells ($1\sim8 \times 10^3$ cells) were processed by using 200 $\mu g \cdot mL^{-1}$ of NP_{PLGA}. The sediments were gathered and washed three times by PBS to eliminate the unabsorbed

NP_{PLGA}. When TMB and H_2O_2 were available in the studied system, the absorbed NP_{PLGA} could catalyze a color reaction that could be discerned by bare eyes and be quantitatively detected the absorbance at 652 nm. When the number of A549 cells raised, the formation of TMB oxidation products changed rapidly, suggesting that more NP_{PLGA} were absorbed by A549 cells. Utilizing this waytechnique, few cells of about 1×10^3 A549 could be detected (Figs. 4A and 4B).

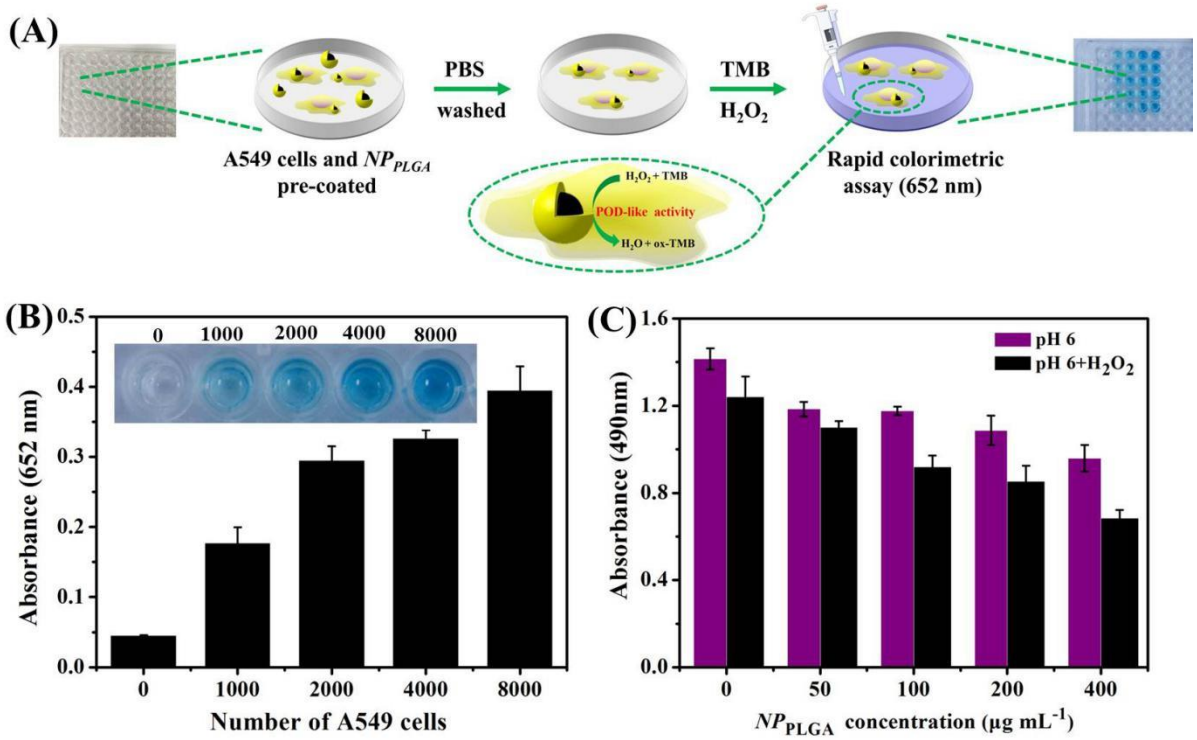

Fig. 4 A Schematic illustrated the process of quantitative colorimetric assay of A549 cells via the POD-like performance of NP_{PLGA}, and **B** A549 cells were detected based on the POD-like activity of NP_{PLGA} in the presence of TMB. Inset: indicates the change of the color related to the various number of A549 cells. **C** The concentration-dependent cytotoxicity assay of NP_{PLGA} in acidic TME.

Furthermore, the cytotoxicity of NP_{PLGA} to A549 cells was determined by MTT assay under acidic TME conditions. In comparison with the NP_{PLGA} treatment, the survival fraction of cells after H_2O_2 treatment under acid TME was significantly reduced (Fig. 4C). The results show that NP_{PLGA}

decomposed H_2O_2 to form •OH under the mild acidic TME of pH 6.0, triggering the production of ROS and further enhancing the toxic effect of H_2O_2 on cells.

To assess the intracellular •OH production, a ROS fluorescence probe DCFH-DA was employed to estimate the intracellular ROS level. Under the acidic TME, the fluorescence of A549 cells was negligible after co-incubation with NP_{PLGA} or DOX-NP_{PLGA}. In contrast, A549 cells treated with NP_{PLGA} under H_2O_2 displayed strong green fluorescence compared, while cells treated with combined DOX-NP_{PLGA} and H_2O_2 were shown a much stronger green fluorescence (Figs. 5 A and B), implying that under the weak acidic TME condition, DOX-NP_{PLGA} and H_2O_2 generated a great quantity of ROS in the cells.

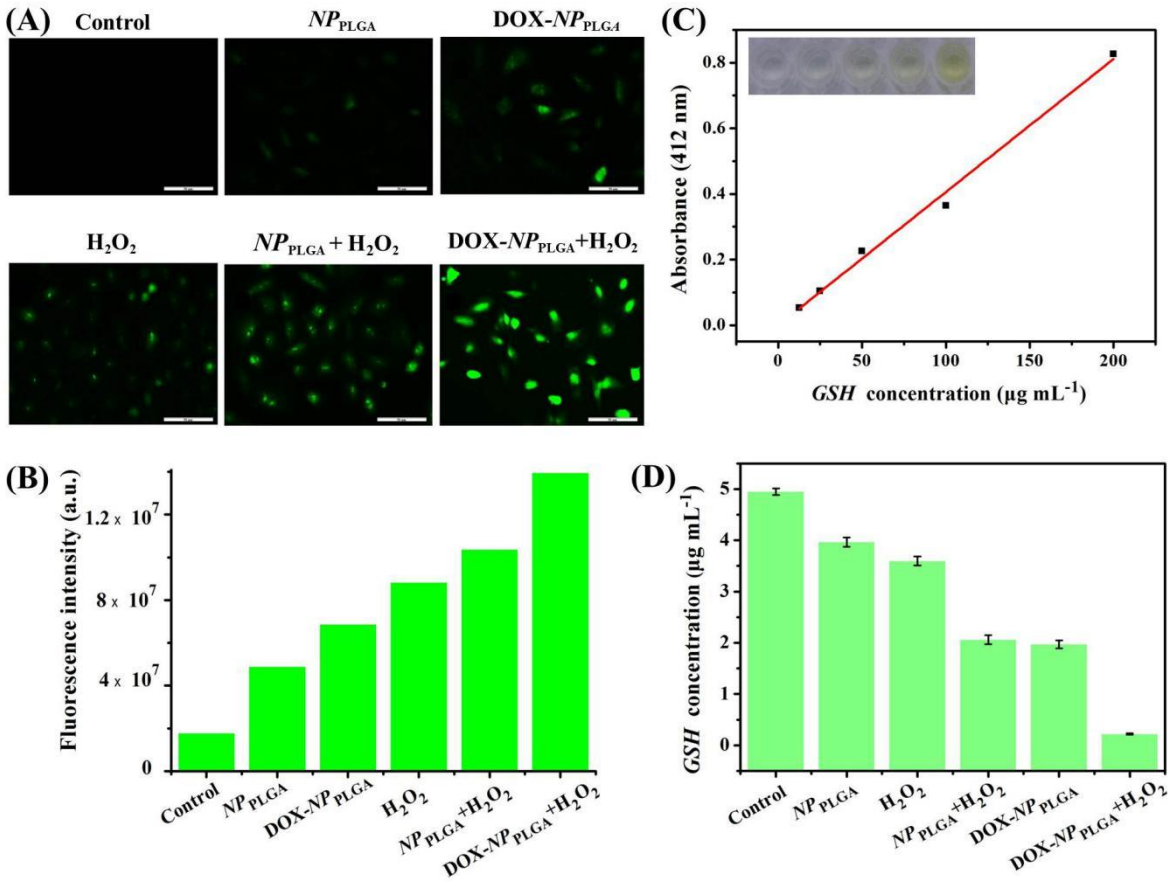

Fig. 5 A Assay of intracellular ROS level, fluorescence images of A549 cells after co-incubation with different formulations for 12 h, and stained using ROS fluorescence probe DCFH-DA, and **B**

corresponding fluorescence intensity analysis. Scale bars =100 μm. **C** A dose-dependent linear curve of various concentrations of GSH solutions with the optimum models, and as well as the inserted photos is the photograph of different concentration. **D** Assay of reduced GSH in the treated A549 cells with different formulations.

GSH protects normal immune system and tissue cells from oxidative damage [48]. Therefore, GSH is an important indicator for studying the effects of ROS, free radicals, and oxides on cells [49]. The results showed that H_2O_2, NP_{PLGA}, NP_{PLGA}+H_2O_2 and DOX-NP_{PLGA} treatment groups all consumed the reduced GSH to varying degrees (Fig. 5D). Moreover, this phenomenon is even more obvious in the DOX-NP_{PLGA} and H_2O_2 co-treated group. These results indicated that the NP_{PLGA} in collaboration with the antineoplastic DOX can significantly consume the reduced GSH in A549 cells, making the tumor cells unable to repair the external oxidative damage, thus increasing the cell death.

We also examined the effect of various concentration DOX-NP_{PLGA} on the cell viability related to the treated A549 cells. According to the Fig. 6A, the cell viability of A549 cells decreased with the rising DOX-NP_{PLGA} concentration. Furthermore, the cell viability of A549 cells processed *via* NP_{PLGA} was much higher than that of the group treated with NP_{PLGA} and H_2O_2, and the cell survival rate of A549 cells treated with DOX-NP_{PLGA} and H_2O_2 was significantly more mitigated compared to the group treated with DOX-NP_{PLGA} (Fig. 6B). These results indicated that the anti-tumor drug DOX could enhance the oxidative damage of NP_{PLGA} to A549 cells under acidic TME conditions, and the combination of the POD-like activity of NP_{PLGA} with DOX could produce a synergistic anti-tumor effect on A549 cells.

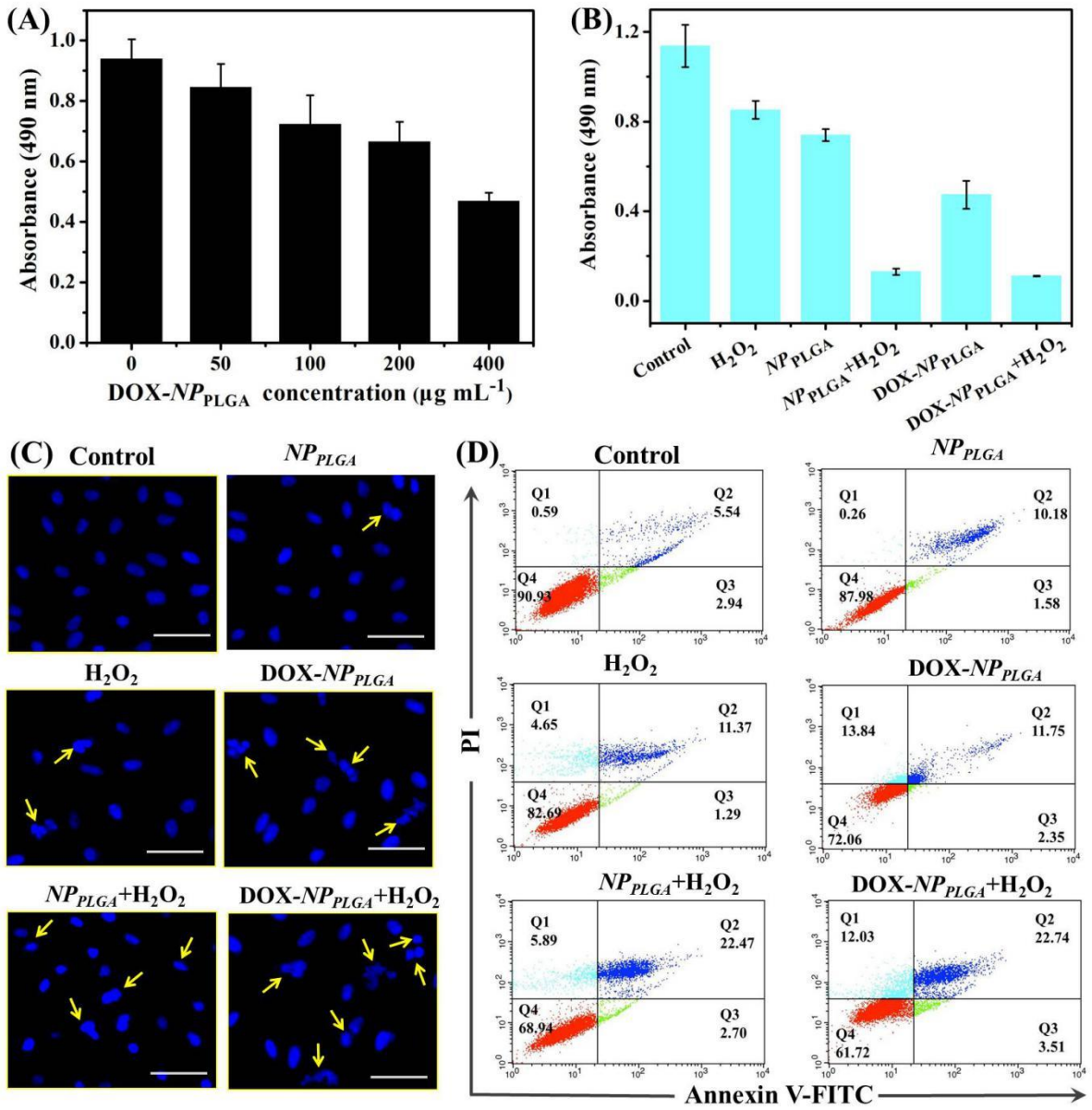

Fig. 6 A Effect of various concentration of DOX-NP_{PLGA} on survival rate of the treated A549 cells. **B** Effect of different formulations on the cell viability of the treated A549. **C** The A549 cells with different formulation treatment under acidic TME (pH 6.0) were stained via Hoechst H33258. Scale bars = 100 μm. **D** Apoptosis assay of the A549 cells with different treatments through flow cytometry by double labeling staining of fluoresce Annexin V-FITC-PI, under acidic TME (pH 6.0). Untreated A549 cells employed as control.

To observe the apoptotic cells' nuclear division, the processed A549 cells were stained with the

fluorescent dye Hoechst H33258, which could combine with the AT-rich zone of DNA to analyze the DNA of apoptotic cells relatively quantitatively [50]. The results showed that when A549 cells were co-treated with DOX-NP_{PLGA} and H_2O_2, the alterations including nuclear peripheral accumulation, chromatin condensation, and nuclear segmentation were considerably greater than those in other groups (Fig. 6C).

In order to further investigate the apoptosis mechanism, flow cytometry was used to quantitatively examination the apoptosis level of the processed A549 cells. The A549 cells were incubated with different formulations including H_2O_2, NP_{PLGA}, NP_{PLGA}+H_2O_2, DOX-NP_{PLGA} and DOX-NP_{PLGA}+H_2O_2 under acidic TME conditions (pH 6.0). The number of cells in each quadrant was quantitatively analyzed. The results showed the apoptosis of A549 cells processed with NP_{PLGA} + H_2O_2 was more obvious compared to the H_2O_2 group, and while the apoptosis of A549 cells with combined DOX-NP_{PLGA} + H_2O_2 treatment was much more obvious, indicating that the A549 cells produced extra high toxicity •OH (Fig. 6D). These results also indicated that nanozyme activity of NP_{PLGA} together with anti-tumor drug DOX could induce apoptosis and enhance anti-tumor effect under mild acidic TME.

Conclusion

In summary, we successfully constructed NP_{PLGA} i.e. PLGA grafted γ-Fe_2O_3 NPs with high dual POD-like and CAT-like activities under different conditions. Under acidic TME conditions, NP_{PLGA} showed POD-like mimetic activity, and could effectively catalyze the decomposition of H_2O_2 to produce high toxicity of •OH through typical Fenton catalytic reaction, leading to lung adenocarcinoma A549 cell death. At the same time, under the neutral TME condition, NP_{PLGA}

exhibited CAT-like simulation activity, and could decompose H_2O_2 to form H_2O and O_2, thereby reducing the oxidative damage of H_2O_2 to lung adenocarcinoma A549 cells. More importantly, NP_{PLGA} of POD-like activity combined with the anti-tumor drug DOX, which can induce the obviously increasing apoptosis rate and enhanced anti-tumor effect for lung adenocarcinoma A549 cells. This present work therefore indicates an essential opportunity towards the development of an effective biomimetic nanoplatform with dual inorganic nanozymes to simulate the catalytic activity of lung tumor treatment.

Acknowledgements

This study was supported by College of Bioengineering, Henan University of Technology; Henan Bioengineering Research Center; Henan Provincial People's Hospital; School of Pharmacy, Henan University.

Authors' contributions

Xueqin Wang presented the idea, supervised the wholework, manuscript modification and fnancial support, Miao Cui, Fan Ouyang, and Yuqi Guo performed experiments, data analysis and interpretation, and the manuscript writing. Ruifang Li, Shaofeng Duan and Tiandi Xiong designed experiments, technical assistance and fnal approval of manuscript. Huiru, Zhang and Yunlong Wang contributed equally to this work. All authors read and approved the final manuscript.

Funding

This work was supported by the China Postdoctoral Science Foundation (No. 2019M652541), Innovation Scientists and Technicians Troop Construction Projects of Henan Province (No. 192101510001), the Scientific and Technological Project of Henan Province (No. 182 102 210 394),

the Young Core Instructor Program in Higher Education Institution of Henan province (No. 2018 GGJS 067), the Young Core Instructor Program from Henan University of Technology (No. 214 200 55). Appendix A. Supplementary data: Supplementary data associated with this article can be found in on-line attachments.

Availability of data and materials

All data and materials are available in the manuscript.

Ethics approval and consent to participate

Not applicable.

Consent for publication

The manuscript has been read and approved by all the named authors.

Competing interests

The authors declare no conflict of interest.

Author details

[1] College of Bioengineering, Henan University of Technology, Zhengzhou, Henan 450001, P.R. China; [2]Henan Bioengineering Research Center, Zhengzhou, 450046, P.R.China; [3]Henan Provincial People's Hospital, Zhengzhou 450003, P.R. China; [4]School of Pharmacy, Henan University, Kaifeng, Henan 475004, P.R. China.

References

1. Gao S, Lin H, Zhang H, Yao H, Chen Y, Shi J. Nanocatalytic tumor therapy by biomimetic dual

inorganic nanozyme-catalyzed cascade reaction. Adv. Sci. 2018;6:1801733.

2. Li SR, Huang YC, Liu JR, Wang EK, Wei H. Nanozymes in analytical chemistry: from in vitro detection to live bioassays. Prog. Biochem. Biophys. 2018;45:129-147.

3. LinY, Ren J, Qu X. Catalytically active nanomaterials: a promising candidate for artificial enzymes. Acc. Chem. Res. 2014;47:1097-105.

4. Kumar S, Bhushan P, Bhattacharya S. Facile synthesis of Au@Ag–hemin decorated reducedgraphene oxide sheets: a novel peroxidase mimetic for ultrasensitive colorimetric detection of hydrogen peroxide and glucose. RSC Adv. 2017;7:37568-77.

5. Fei H, Dong J, Feng Y, Allen CS, Wan C, Volosskiy B, Li M, Zhao Z, Wang Y, Sun H, An P, Chen W, Guo Z, Lee C, Chen D, Shakir I, Liu M, Hu T, Li Y, Kirkland AI, Duan X, Huang Y. General synthesis and definitive structural identification of MN_4C_4 single-atom catalysts with tunable electrocatalytic activities. Nat. Catal. 2018;1:63.

6. Zhang Z, Zhang X, Liu B, Liu J. Molecular imprinting on inorganic nanozymes for hundred-fold enzyme specificity. J. Am. Chem. Soc. 2017;139:5412-19.

7. Wu L, Wan G, Hu N, He Z, Shi S, Suo Y, Wang K, Xu X, Tang Y, Wang G. Synthesis of porous $CoFe_2O_4$ and its application as a peroxidase mimetic for colorimetric detection of H_2O_2 and organic pollutant degradation. Nanomaterials. 2018;8:451.

8. Tian R, Sun J, Qi Y, Zhang B, Guo S, Zhao M. Inflfluence of VO_2 nanoparticle morphology on the colorimetric assay of H_2O_2 and glucose. Nanomaterials. 2017;7:347.

9. Vallabani NV, Karakoti AS, Singh S. ATP-mediated intrinsic peroxidase-like activity of Fe_3O_4-based nanozyme: One step detection of blood glucose at physiological pH. Colloids Surf. B Biointerfaces. 2017;153:52-60.

10. Wu J, Li S, Wei H. Integrated nanozymes: facile preparation and biomedical applications. Chem. Commun. 2018;54:6520-30.

11. Zhou Y, Liu B, Yang R, Liu J. Filling in the gaps between nanozymes and enzymes: challenges and opportunities. Bioconjugate. Chem. 2017;28:2903-09.

12. Mahmoudi M, Simchi A, Imani M, Hafeli OU. Superparamagnetic iron oxide nanoparticles with rigid cross-linked polyethylene glycol fumarate coating for application in imaging and drug delivery. J. Phys. Chem. C. 2009;113:8124-31.

13. Tang C, He Z, Liu H, Xu Y, Huang H, Yang G, Xiao Z, Li S, Liu H, Deng Y, Chen Z, Chen H, He N. Application of magnetic nanoparticles in nucleic acid detection. J. Nanobiotechnol. 2020;18:62.

14. Zhu F, Tan G, Zhong Y, Jiang Y, Cai L, Yu Z, Liu S, Ren F. Smart nanoplatform for sequential drug release and enhanced chemo-thermal effect of dual drug loaded gold nanorod vesicles for cancer therapy. J. Nanobiotechnol. 2019;17:44.

15. Chung HT, Hsiao KJ, Hsu CS, Yao M, Chen CY, Wang WS, Huang MD. Iron oxide nanoparticle-induced epidermal growth factor receptor expression in human stem cells for tumor therapy. Acs Nano. 2011;5:9807.

16. Zhu L, Zhou Z, Mao H, Yang L. Magnetic nanoparticles for precision oncology: theranostic magnetic iron oxide nanoparticles for image-guided and targeted cancer therapy. Nanomedicine (Lond). 2017;12:73-87.

17. Soares PIP, Laia TAC, Carvalho A, Pereira CL, Coutinho TJ, Ferreira MI, Borges PJ. Iron oxide nanoparticles stabilized with a bilayer of oleic acid for magnetic hyperthermia and MRI applications. Appl. Surf. Sci. 2016;383:240-247.

18. Hemalatha T, Prabu P, Gowthaman KM. Fabrication and characterization of dual acting oleyl chitosan functionalised iron oxide/gold hybrid nanoparticles for MRI and CT imaging. Int. J. Bio. Macromol. 2018;112:250-257.

19. Olsvik O, Popovic T, Skjerve E, Cudjoe SK, Hornes E, Ugelstad J, Uhlen M. Magnetic separation techniques in diagnostic microbiology. Clin. Microbiol. Rev. 1994;7:43.

20. Gupta KA, Curtis GSA. Lactoferrin and ceruloplasmin derivatized superparamagnetic iron oxide nanoparticles for targeting cell surface receptors. Biomaterials. 2004;25:3029-40.

21. Gupta KA, Curtis GSA. Lactoferrin and ceruloplasmin derivatized superparamagnetic iron oxide nanoparticles: preparation, characterization and their influence on human dermal fibroblasts in culture. Proc. 30th Annu. Symp. Controlled Release Bioact. Mater. 2003;30:788.

22. Min C, Shao H, Liong M, Yoon JT, Weissleder R, Lee H. Mechanism of magnetic relaxation switching sensing. ACS Nano. 2012;6:6821-28.

23. Cheon J, Lee HJ. Synergistically integrated nanoparticles as multimodal probes for nanobiotechnology. Acc.Chem. Res. 2008;41:1630-40.

24. Ebrahimisadr S, Aslibeiki B, Asadi R. Magnetic hyperthermia properties of iron oxide nanoparticles: the effect of concentration. Physica C. 2018;549:119-21.

25. Espinosa A, Di RC, Kolosnjaj-Tabi J, Flaud P, Pellegrino T, Wilhelm C. Duality of iron oxide nanoparticles in cancer therapy: amplification of heating efficiency by magnetic hyperthermia and photothermal bimodal treatment. ACS Nano. 2016;10:2436-46.

26. Chen Z, Yin JJ, Zhou YT, Zhang Y, Song L, Song M, Hu S, Gu N. Dual enzyme-like activities of iron oxide nanoparticles and their implication for diminishing cytotoxicity. ACS Nano. 2016;6:4001-12.

27. Pisanic RT, Blackwell DJ, Shubayev IV, Finones RR, Jin S. Nanotoxicity of iron oxide nanoparticle internalization in growing neurons. Biomaterials. 2007;28:2572-81.

28. Gao L, Zhuang J, Nie L, Zhang J, Zhang Y, Gu N, Wang T, Feng J, Yang D, Perrett S, Yan X. Intrinsic peroxidase-like activity of ferromagnetic nanoparticles. Nat. Nanotech. 2007;2:577-83.

29. Duesterberg CK, Mylon SE, David WT. pH effects on iron-catalyzed oxidation using Fenton's reagent. Environ. Sci. Technol. 2008;42:8522-27.

30. Kang YS, Risbud S, Rabolt JF, Stroeve P. Synthesis and characterization of nanometer-size Fe_3O_4 and γ-Fe_2O_3 particles. Chem. Mater. 1996;8:2209-11.

31. Chen Z, Yin JJ, Zhou TY, Zhang Y, Song L, Song M, Gu N. Dual enzyme-like activities of iron oxide nanoparticles and their implication for diminishing cytotoxicity. ACS Nano. 2012;6:4001-12.

32. Song L, Huang C, Zhang W, Ma M, Chen Z, Gu N, Zhang Y. Graphene oxide-based Fe_2O_3 hybrid enzyme mimetic with enhanced peroxidase and catalase-like activities. Colloid. Surf. A 2016;506:747-55.

33. Niu YH, Zhang D, Zhang XS, Zhang LX, Meng FZ, Cai QY. Humic acid coated Fe_3O_4 magnetic nanoparticles as highly efficient fenton-like catalyst for complete mineralization of sulfathiazole. J. Hazard. Mater. 2011;190:559-65.

34. Wang N, Zhu HL, Wang LD, Wang QM, Lin FZ, Tang QH. Sono-assisted preparation of highly-efficient peroxidase-like Fe_3O_4 magnetic nanoparticles for catalytic removal of organic pollutants with H_2O_2. Ultrason. Sonochem. 2010;17:526-33.

35. Shin S, Yoon H, Jang J. Polymer-encapsulated iron oxide nanoparticles as highly efficient fenton catalysts. Catal. Commun. 2008;10:178-82.

36. Fan J, Yin JJ, Ning B, Wu X, Hu Y, Ferrari M, Anderson JG, Wei J, Zhao Y, Nie G. Direct evidence for catalase and peroxidase activities of ferritin-platinum nanoparticles. Biomaterials. 2011;32:1611-18.

37. Dickinson BC, Chang CJ. Chemistry and biology of reactive oxygen species in signaling or stress responses. Nat. Chem. Biol. 2011;7:504.

38. Wang F, Ju E, Guan Y, Ren J, Qu X. Light-mediated reversible modulation of ROS level in living cells by using an activity-controllable nanozyme. Small. 2017;13:1603051.

39. Zhao J, Cai X, Gao W, Zhang L, Zou D, Zheng Y, Li Z, Chen H. Prussian blue nanozyme with multienzyme activity reduces colitis in mice. ACS Appl. Mater. Interfaces. 2018;10:26108.

40. Gao S, Jin Y, Ge K, Li Z, Liu H, Dai X, Zhang Y, Chen S, Liang X, Zhang J. Self-Supply of O_2 and H_2O_2 by a nanocatalytic medicine to enhance combined chemo/chemodynamic therapy. Adv. Sci. 2019;6:1902137.

41. Chen Q, Luo Y, Du W, Liu Z, Zhang S, Yang J, Yao H, Liu T, Ma M, Chen H. Clearable theranostic platform with a pH-independent chemodynamic therapy enhancement strategy for synergetic photothermal tumor therapy. ACS Appl. Mater. Interfaces. 2019;11:18133-44.

42. Qu S, Yang H, Ren D, Kan S, Zou G, Li D. Magnetite nanoparticles prepared by precipitation from partially reduced ferric chloride aqueous solutions. J. Colloid Interface Sci. 1999;215:190-92.

43. Sun YK, Ma M, Zhang Y, Gu N. Synthesis of nanometer-size maghemite particles from magnetite. Colloid. Surf. A 2004;245:15-19.

44. Wang X, Ou Y, Cui L, Xiong T, Guan X, Guo Y, Duan S. Surface coating-modulated peroxidase-like activity of maghemite nanoparticles for a chromogenic analysis of cholesterol. J

Nanopart Res. 2019;21:1-13.

45. Dong YL, Zhang HG, Rahman ZU, Su L, Chen XJ, Hu J. Graphene oxide-Fe_3O_4 magnetic nanocomposites with peroxidase-like activity for colorimetric detection of glucose. Nanoscale. 2012;4:3969.

46. Singh S. Cerium oxide based nanozymes: redox phenomenon at biointerfaces. Biointerphases. 2016;11:04B202.

47. Giorgio M, Trinei M, Migliaccio E, Pelicci GP. Hydrogen peroxide: a metabolic by-product or a common mediator of ageing signals? Nat. Rev. Mol. Cell Biol. 2007;8:722-28.

48. Han BY, Yuan JP, Wang EK. Sensitive and selective sensor for biothiols in the cell based on the recovered fluorescence of the CdTe quantum dots-Hg (II) system. Anal. Chem. 2009;81:5569-73.

49. Pastore A, Federici G, Bertini E, Piemonte F. Analysis of glutathione: implication in redox and detoxification. Clin. Chim. Acta. 2003;333:19-39.

50. Chamaon K, Stojek J, Kanakis D, Braeuninger S, Kirches E, Krause G, Mawrin C, Dietzmann K. Micromolar concentrations of 2-methoxyestradiol kill glioma cells by an apoptotic mechanism, without destroying their microtubule cytoskeleton. J. Neuro-Oncol. 2005;72:11-16.

Figures

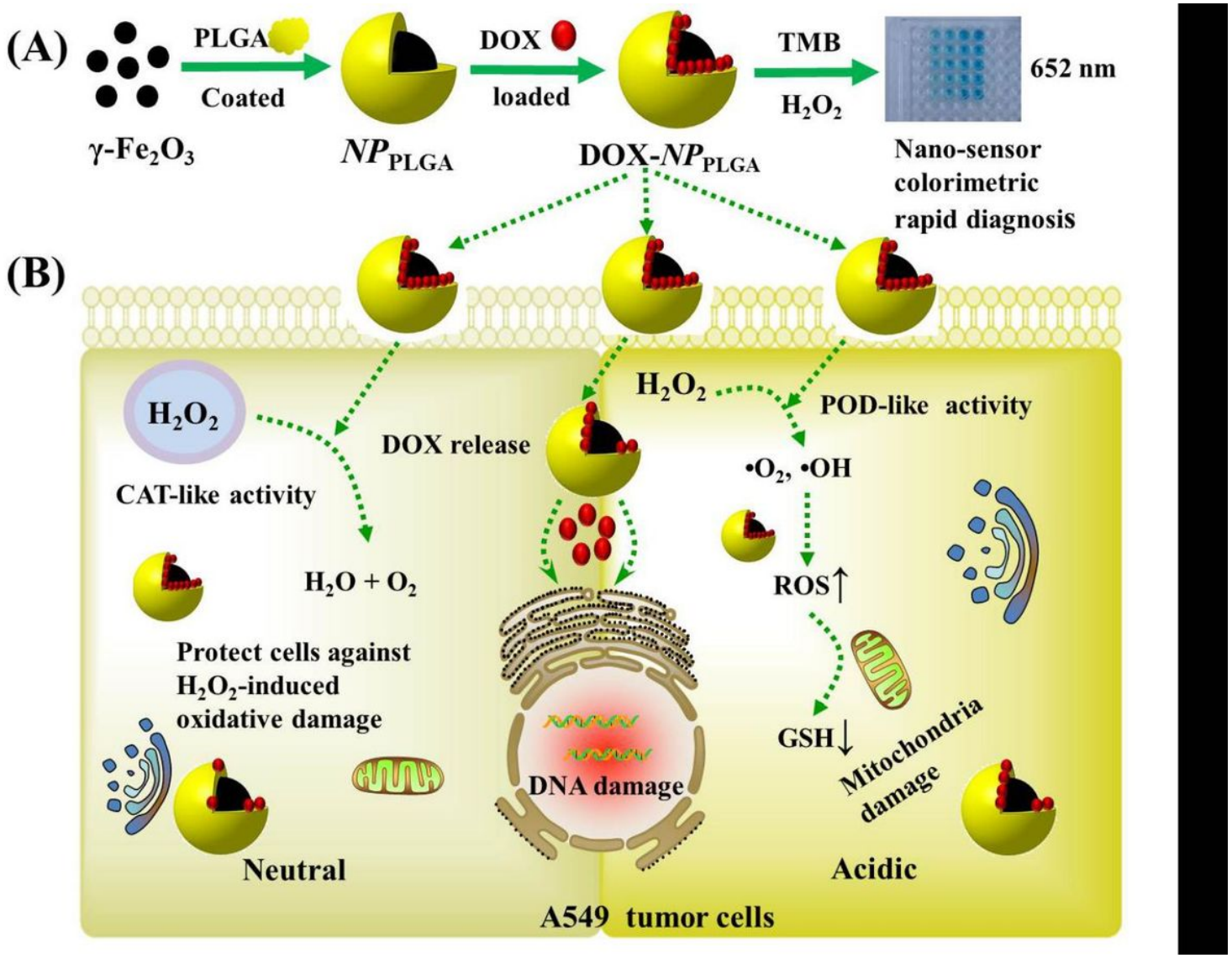

Figure 1

Schematic diagram of the functional pattern of DOX-NPPLGA and its enhanced anti-tumor effect. A Preparation of DOX-loaded NPPLGA and colorimetric determination in lung adenocarcinoma A549 cells. B In a neutral TME, DOX-NPPLGA displayed CAT-like activity by decomposing H2O2 into H2O and O2. In an acidic TME, DOX-NPPLGA released DOX and exhibited POD-like activity to produce highly toxic •OH, which caused the growth of ROS accumulation as well as the decrease of GSH in tumor A549 cells, and the further synergistic effect with DOX, causing efficient cell death.

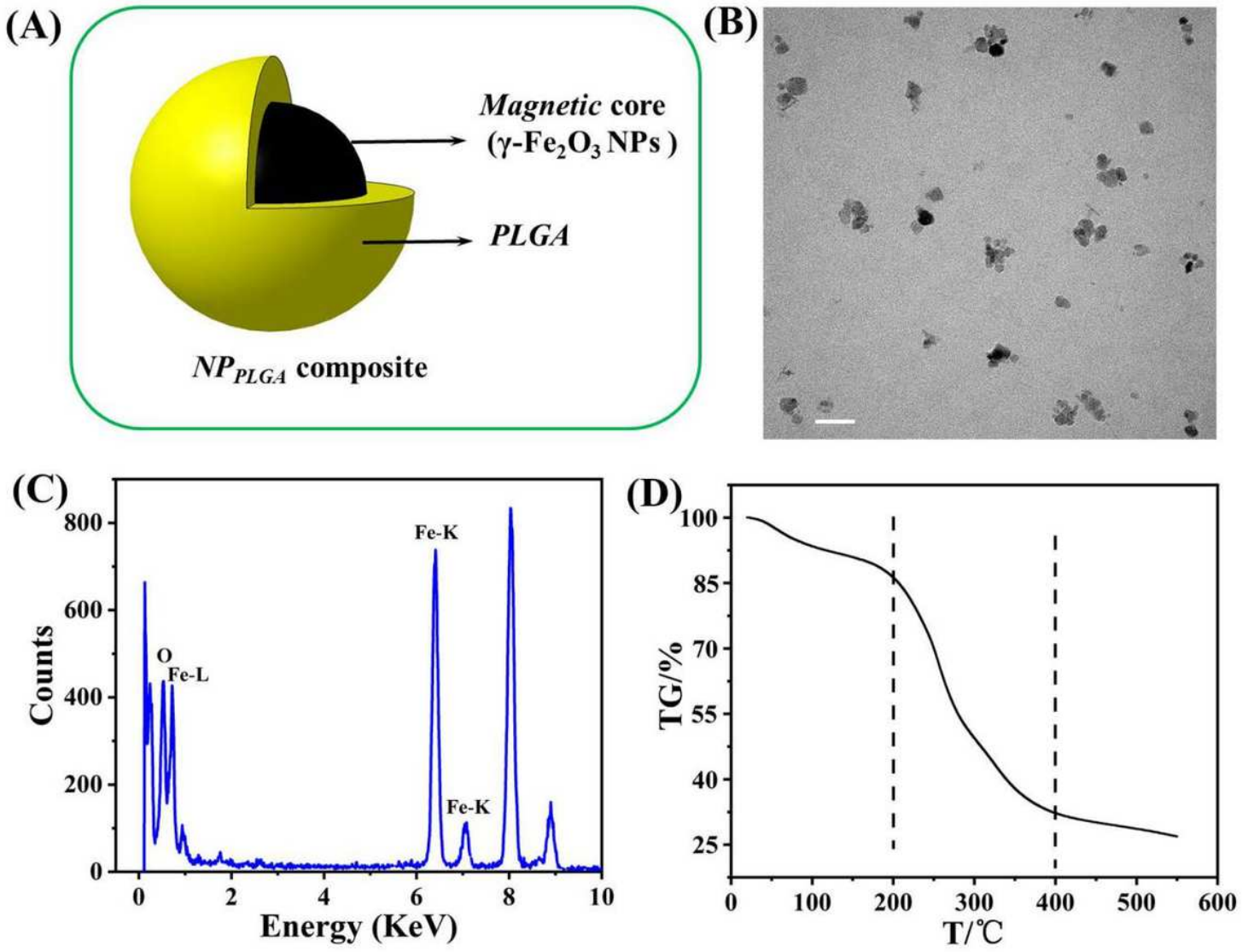

Figure 2

1 A Schematic illustration of the composite NPPLGA. B TEM image of NPPLGA. Scale bar = 50 nm. C EDS spectrum of NPPLGA. D Thermogravimetric curve of NPPLGA.

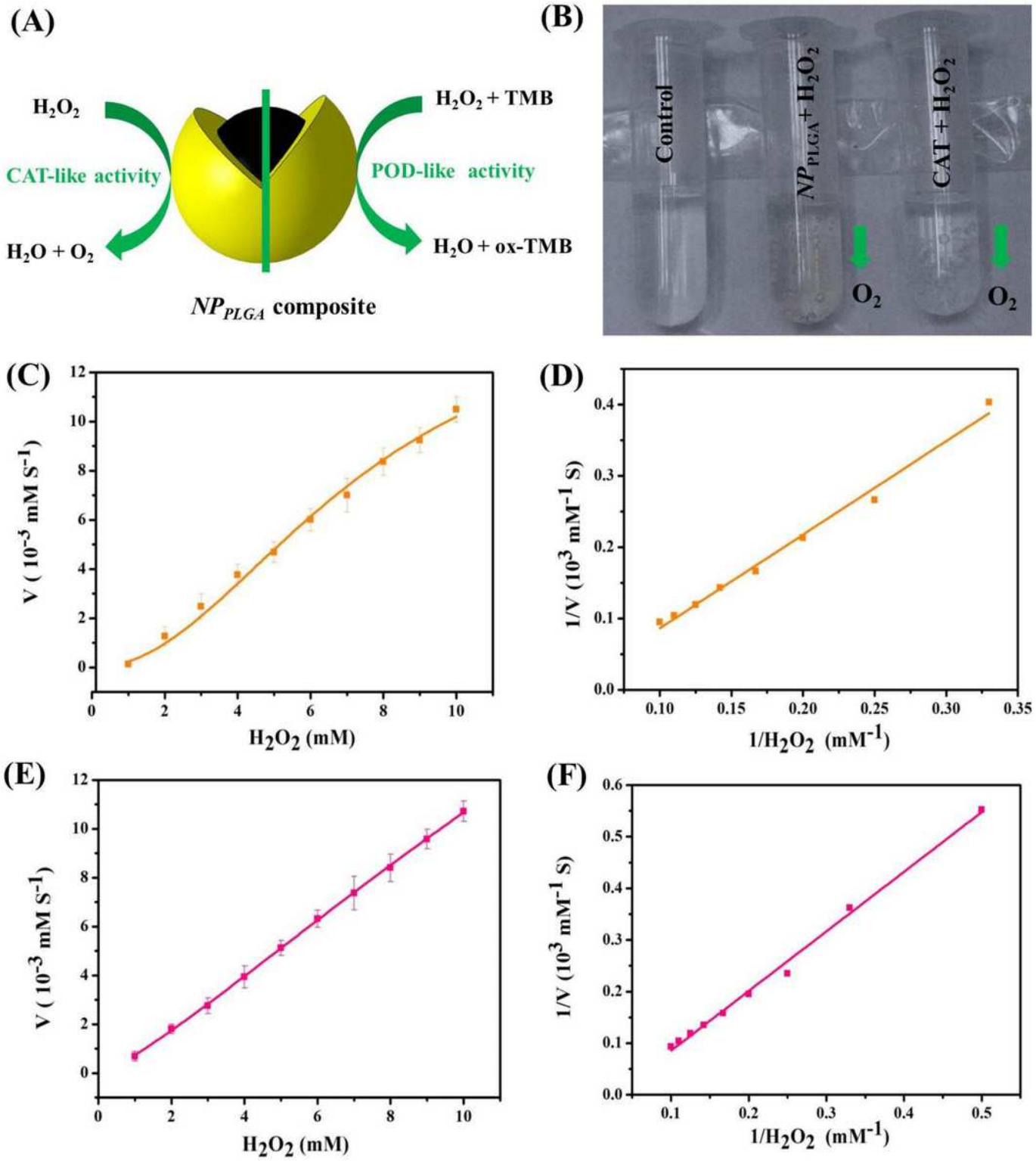

Figure 3

A Schematic illustration for dual enzyme-like catalytic performance of the NPPLGA. B CAT-like activity assay of NPPLGA, both NPPLGA and natural CAT can catalyze H2O2 to produce O2 when H2O2 is available in the system. C Steady-state Kinetic assays for NPPLGA in the presence of H2O2, and D corresponding double-reciprocal plot. E) Kinetic assays of natural CAT in the presence of H2O2, and F) corresponding double-reciprocal plot.

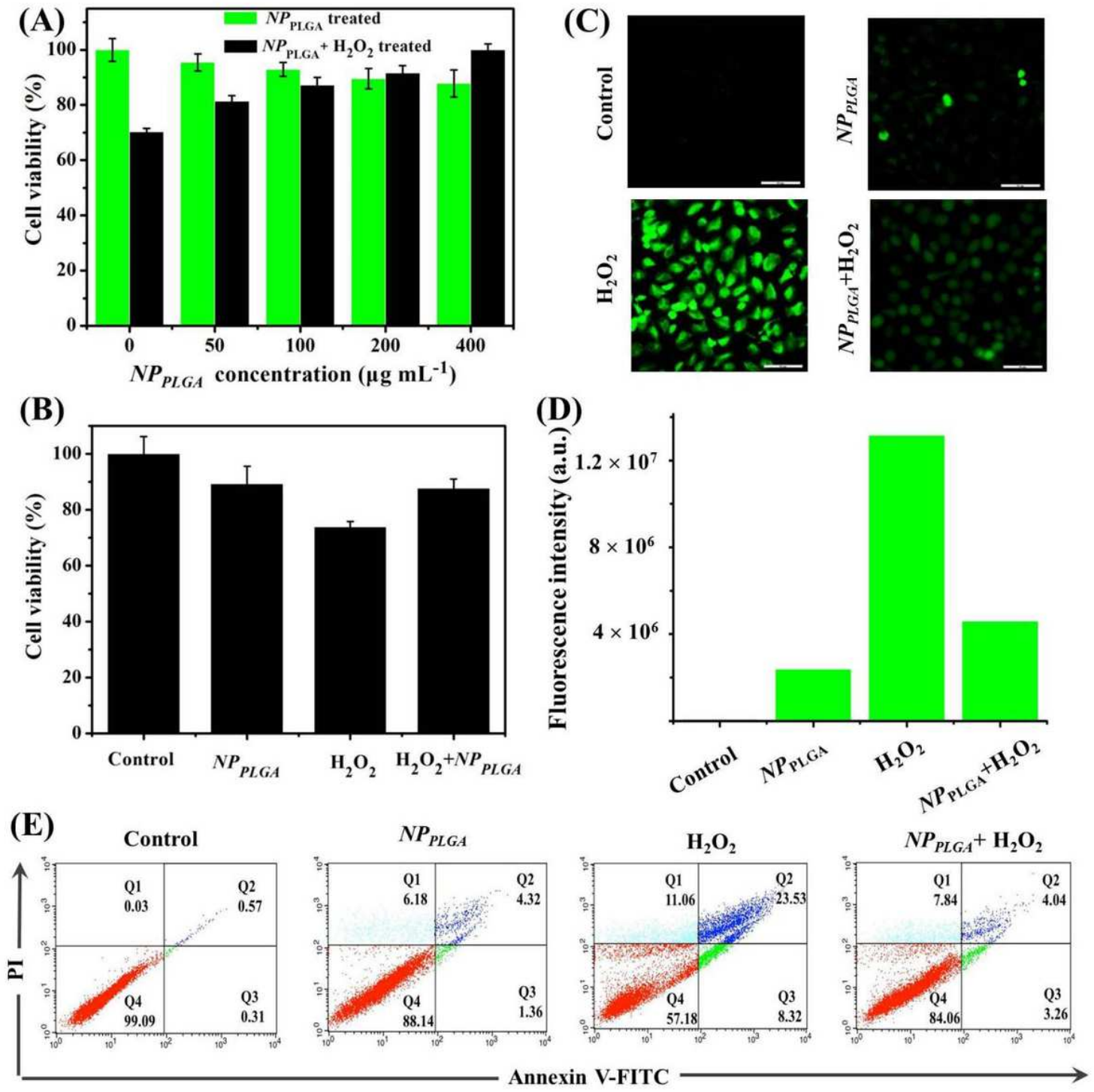

Figure 4

A Cytotoxicity of NPPLGA and H2O2-induced oxidative damage assays of treated A549 cells with various concentration of NPPLGA including 50, 100, 200, 400 μg·mL-1, and the cells were treated with various concentration NPPLGA and 5 mM H2O2 under neutral TME conditions (pH 7.4). B H2O2-induced oxidative damage of A549 cells with different formulation treatments, the cells were treated for 12h, and the concentration of NPPLGA was 200 μg·mL-1. C Assays of ROS production in treated A549 cells for 12 h with different formulations, and D corresponding statistical of the fluorescence intensity analysis in the

processed cells. E Apoptosis assays of the processed A549 cells with different treatment through flow cytometry utilizing the staining methods of fluorescein Annexin V-FITC-PI double labeling, untreated A549 cells employed as a control. Early apoptosis (bottom right), late apoptosis (upper right), necrotic cells (upper left), and normal cells (bottom left).

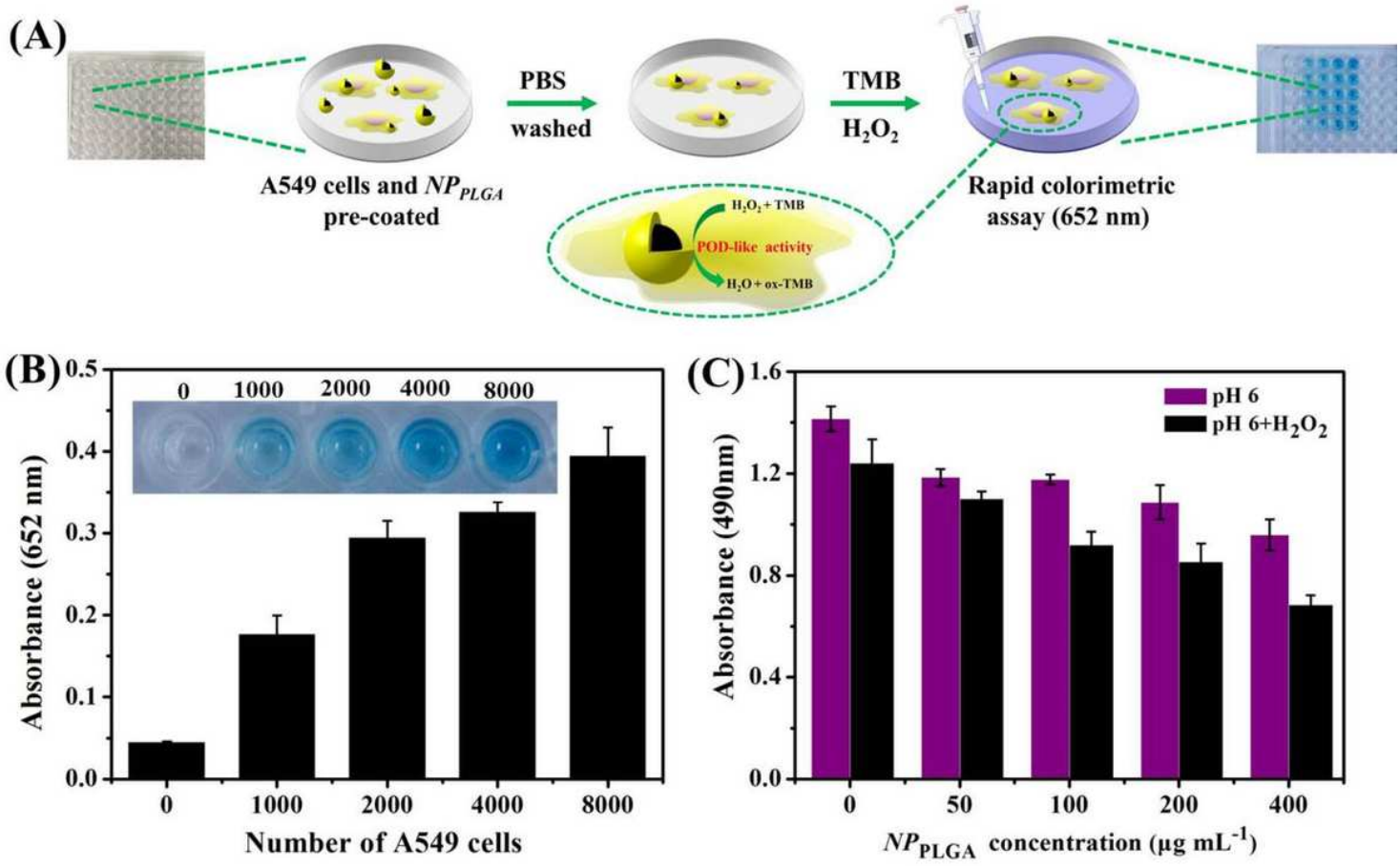

Figure 5

A Schematic illustrated the process of quantitative colorimetric assay of A549 cells via the POD-like performance of NPPLGA, and B A549 cells were detected based on the POD-like activity of NPPLGA in the presence of TMB. Inset: indicates the change of the color related to the various number of A549 cells. C The concentration-dependent cytotoxicity assay of NPPLGA in acidic TME.

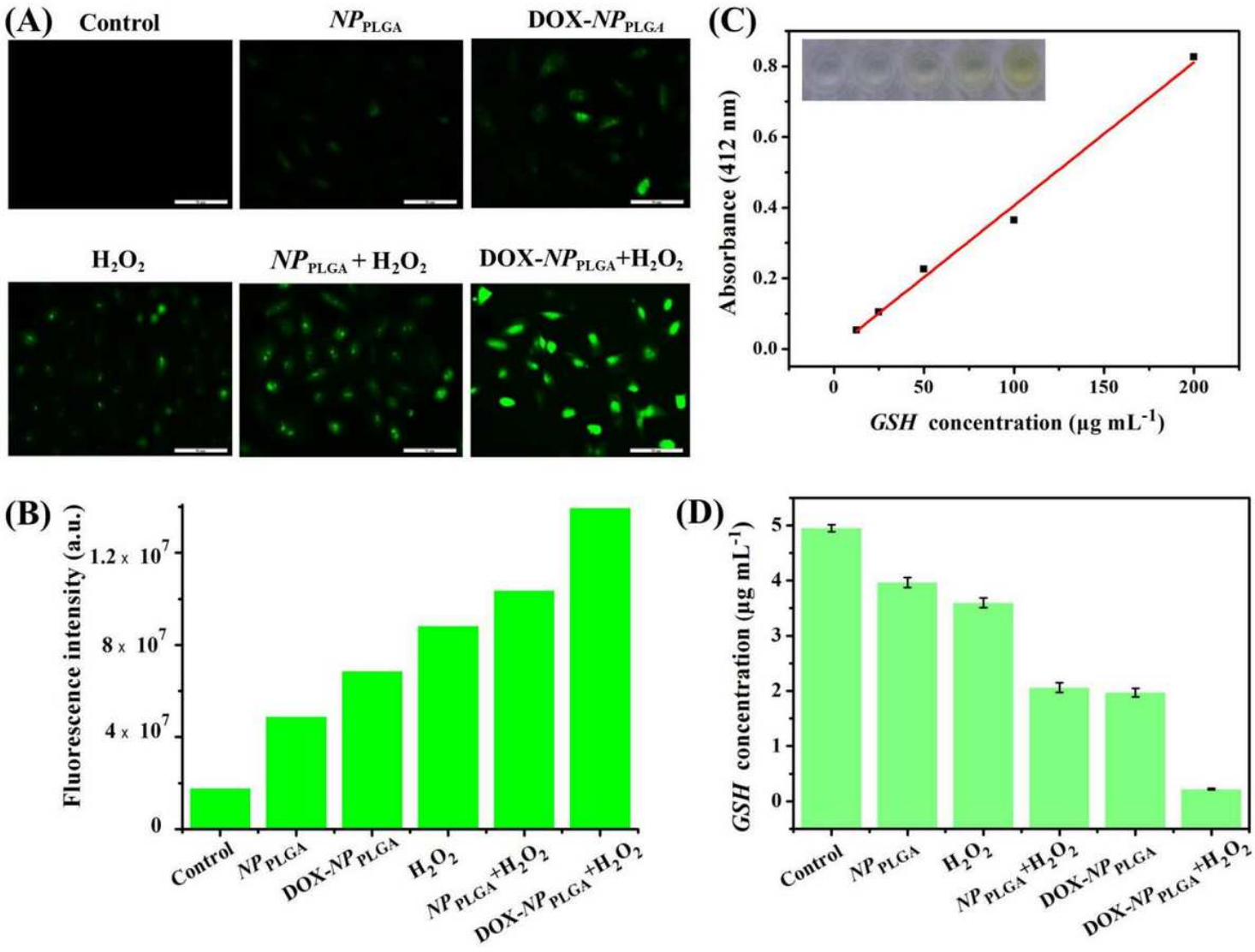

Figure 6

A Assay of intracellular ROS level, fluorescence images of A549 cells after co-incubation with different formulations for 12 h, and stained using ROS fluorescence probe DCFH-DA, and B corresponding fluorescence intensity analysis. Scale bars =100 μm. C A dose-dependent linear curve of various concentrations of GSH solutions with the optimum models, and as well as the inserted photos is the photograph of different concentration. D Assay of reduced GSH in the treated A549 cells with different formulations.

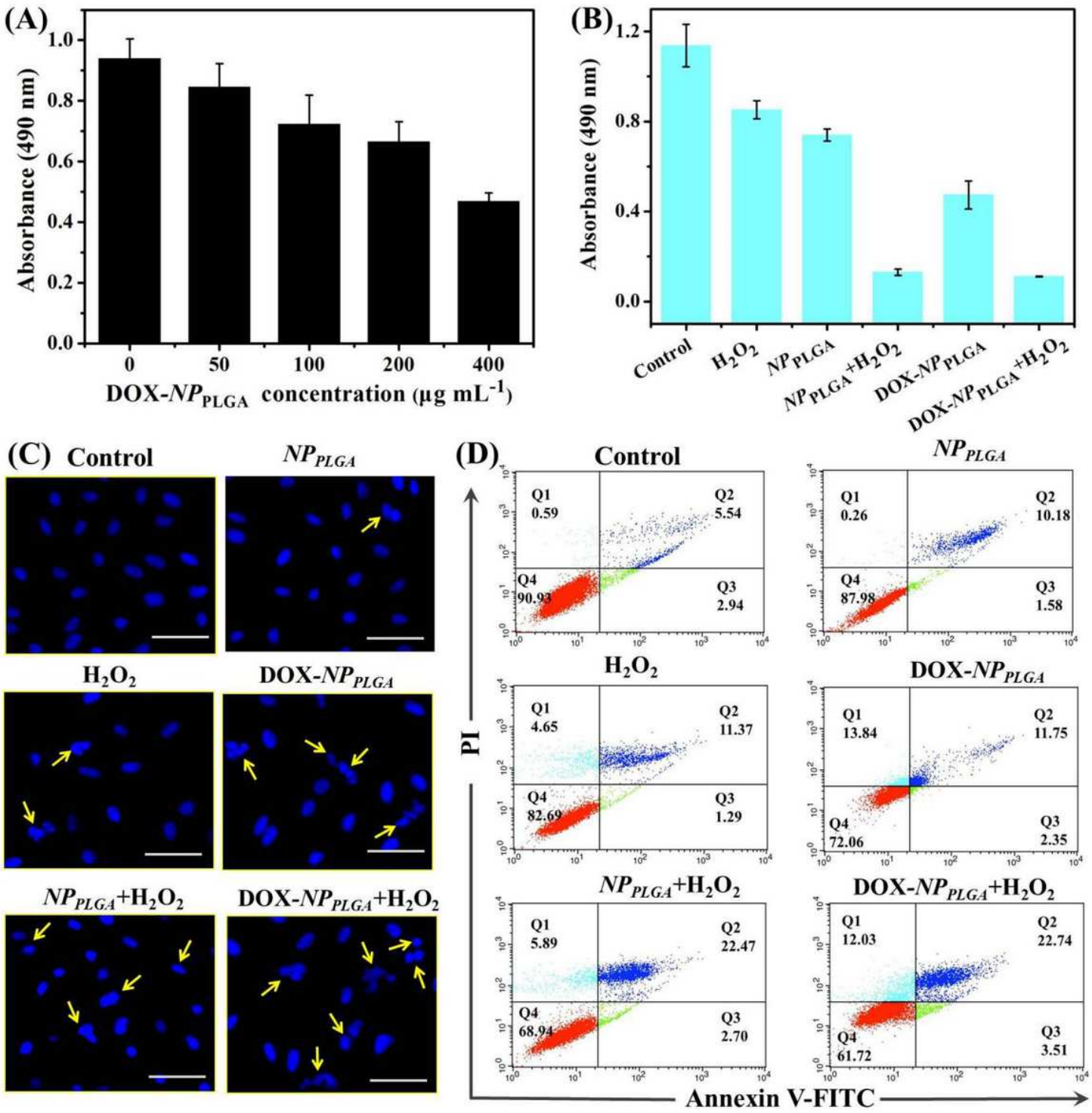

Figure 7

A Effect of various concentration of DOX-NPPLGA on survival rate of the treated A549 cells. B Effect of different formulations on the cell viability of the treated A549. C The A549 cells with different formulation treatment under acidic TME (pH 6.0) were stained via Hoechst H33258. Scale bars = 100 μm. D Apoptosis assay of the A549 cells with different treatments through flow cytometry by double labeling staining of fluoresce Annexin V-FITC-PI, under acidic TME (pH 6.0). Untreated A549 cells employed as control.